

Molecular Imaging of Macroheterocycles for Demonstration of Classical Nucleation and Quantum Switching

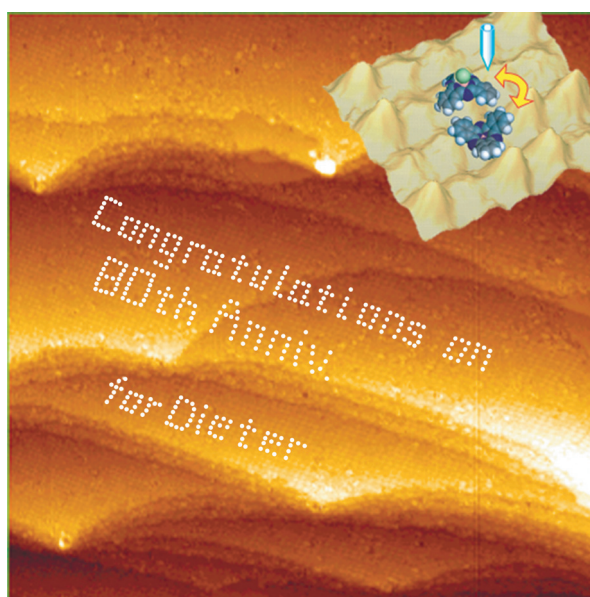
Hisao Yanagi

Graduate School of Science and Technology, Nara Institute of Science and Technology, 8916-5 Takayama, Ikoma, 630-0192 Nara, Japan
E-mail: yanagi@ms.naist.jp

Dedicated to Professor Dieter Wöhrle on the occasion of his Birthday

Single molecular imaging by scanning tunneling microscopy (STM) was carried out for platinum tetra(3,5-di-tert-butylphenyl)porphyrin (Pt-TBPP) and chloro[subphthalocyaninato]boron(III) (SubPc) adsorbed on Cu (001) surface under ultrahigh vacuum. In the former, two-dimensional nucleation growth of Pt-TBPP assemblies was demonstrated according to classical thermodynamic mechanism. The registry of Pt-TBPP molecules into the kink sites minimized the free energy for nucleation resulting in formation of singular nuclei with rectangular shapes. In the latter, STM-induced flip-flop switching was molecularly visualized for epitaxially adsorbed SubPc arrays. The asymmetric SubPc molecules initially adsorbed with its axial chlorine atom either upwards or downwards. After scanning at a negative bias, the upward molecules turn upside down while all molecules switched to the upward orientation at a positive bias. This orientational switching is not consistent with that expected from the polarity of the SubPc molecule along the Cl-B bond. Moreover, similar switching phenomena were observed during continuous scanning at a constant bias. Molecular energy calculation and statistical thermodynamic evaluation concluded that the tip-triggered fluctuation in the close-packed SubPc array induced the molecular rearrangement with stochastic flip-flop switching. This stochastic behavior suggests that the switching is not a single molecular event but is more related to intermolecular entanglement among arrayed molecules which envisages us to consider molecular-based quantum phenomena.

Keywords: Scanning tunneling microscopy, porphyrin, subphthalocyanine, nucleation, molecular switching.



Молекулярная визуализация макрогетероциклов для демонстрации классической нуклеации и квантового переключения

Х. Янаги

Высшая школа науки и технологии, Институт науки и технологий Нары, 8916-5 Такаяма, Икома, 630-0192 Нара, Япония

С помощью сканирующей туннельной микроскопии (СТМ) выполнена мономолекулярная визуализация для тетра(3,5-ди-*tert*-бутилфенил)порфирина платины (Pt-TBPP) и субфталоцианината хлорида бора(III) (SubPc), адсорбированных на поверхности Cu (001) под сверхвысоким вакуумом. Ранее, в соответствии с классическим термодинамическим механизмом был показан рост двумерной нуклеации агрегатов Pt-TBPP. Регистрация молекул Pt-TBPP в местах изломов сводит к минимуму свободную энергию нуклеации, что приводит к образованию единичных зародышей кристаллизации прямоугольной формы. В последнем случае СТМ-индуцированное «flip-flop» переключение было визуализировано для эпитаксиально адсорбированных массивов SubPc на молекулярном уровне. Асимметричные молекулы SubPc первоначально адсорбируются таким образом, что аксиальный атом хлора ориентирован или вверх, или вниз. После сканирования при отрицательном смещении молекулы поворачиваются аксиальным атомом вниз, при положительном смещении – вверх. Это ориентационное переключение не согласуется с ожидаемым от полярности молекулы SubPc вдоль связи Cl-B. Кроме того, подобные явления переключения наблюдались при непрерывном сканировании при постоянном смещении. Расчет молекулярной энергии и статистическая термодинамическая оценка позволили сделать вывод о том, что *tip*-триггерные колебания в плотноупакованном массиве SubPc вызывают молекулярную перестройку со стохастическим «flip-flop» переключением. Такое стохастическое поведение говорит о том, что переключение не является единичным молекулярным событием, а в большей степени связано с межмолекулярным переплетением между массивами молекул, что предполагает рассмотрение квантовых явлений на молекулярном уровне.

Ключевые слова: Сканирующая туннельная микроскопия, порфирин, субфталоцианин, нуклеация, молекулярное переключение.

Introduction

Real imaging of individual molecules has been first demonstrated for chlorinated copper phthalocyanine (CuPcCl₁₆) using high-resolution transmission electron microscopy (HRTEM) by Uyeda *et al.* in 1972.^[1] Computing simulation by the multislice method^[2] proved that the obtained four-lobed image was identified as a projection of piled Pc molecules along a column perpendicular to the specimen film. Further improvement of imaging conditions such as acceleration voltage, lens aberration, focusing parameters and specimen thickness realized atomic resolution to discriminate the central Cu and peripheral Cl atoms in CuPcCl₁₆.^[3] Even though the HRTEM is still a powerful technique for molecular imaging at highest resolution, it is challenging to observe single molecular events due to a sample damage by the electron beam and a low contrast, in particular for organic compounds.^[4,5] As an alternative method for atomic-resolution imaging, scanning tunneling microscopy (STM) has been developed^[6] and its derivative scanning probe microscopy techniques have been widely used for a variety of nanoscale materials and characterization.^[7–11]

The STM methodology has not only accelerated direct imaging of adsorbed molecules on conductive surfaces but also enabled manipulation of individual atoms and molecules,^[12–14] as well as subsequent studies to control chemical reactions and physical properties of molecules.^[15–17] Conformational identification and manipulation of macroheterocycles by STM have been attained for Cu-tetra(3,5-di-*tert*-butylphenyl)porphyrin (Cu-TBPP) adsorbed on a Cu (001) surface at room temperature.^[18,19] The moderate interaction between the four di-*tert*-butylphenyl (*tBP*) groups and Cu surface made a controllable motion of molecules possible with the STM probe. This molecule was also provided to demonstrate conductance switching by rotating the *tBP* group under low-temperature STM manipulation.^[20] Moreover, the peripheral substitution of metal-free TBPP (H₂-TBPP) with cyano groups dramatically changed intermolecular interactions resulting in controlled assembling from monomers to tetramers or one-dimensional (1D) wires^[21] and orientational ordering into two-dimensional (2D) islands.^[22] According to those previous STM studies, the TBPP species is chosen as one of most prosperous macroheterocycles for bottom-up assembling from single molecules to molecular solids. The STM imaging of TBPPs

enables us to directly see how the molecules are dynamically assembled from molecular aggregates to higher dimensional crystals. In the first section, this review presents molecularly resolved nucleation dynamics of TBPP aggregates on Cu surface.^[23] Classical thermodynamics and STM-imaging clearly demonstrate the formation of critical nuclei from two-dimensional gas molecules on the surface.

Another feasibility of STM is scanning probe storage based on bistability of single molecules which leads to a high-density memory on the order of 10 Tbit·cm⁻². Some molecular systems have been provided for switching of individual molecular states by localized tip stimuli.^[24,25] For single-molecular accessibility in the STM-based switching memory, it is required to arrange individual molecules with a moderately isolated space on conductive surfaces. In order to carry out such a bistable molecular alignment, the author chose chloro[subphthalocyaninato]boron(III) (SubPc)^[26] in the second section of this review. The SubPc molecule has a three-fold symmetry shuttlecock structure capable of anisotropic switching between up and down orientations of its axial B-Cl bond. From a standpoint of symmetry matching of molecule-substrate interactions, a well-defined Si (111)-7×7 reconstructed surface was first used for the deposition of SubPc molecules by molecular-beam epitaxy.^[27] A three-lobed STM image corresponding to the SubPc molecule with Cl-down orientation was observed on a specific site of the Si surface in which the inactive Cl head is anchored onto one Si rest atom and the threefold aza-nitrogens sit close to the surrounding Si adatoms. The molecules adsorbed otherwise were chemically dissociated into low-molecular component due to electrophilic attack of the Si dangling bonds. Owing to such an active surface interaction, therefore, the orientational switching of SubPc was not attained on the Si substrate. On the other hand, free-electron surfaces of metals like Ag (111) leave adsorbed SubPc molecules intact and free to move on the surface under thermodynamic equilibrium between the 2D gas phase and self-assembled islands.^[28] As a result, the low diffusion barrier of SubPc molecules on

the symmetry-matched Ag (111) surface makes the STM-switching difficult.

By contrast, the SubPc molecules deposited on the Cu (001) surface are well-ordered into a monolayer array in which the axial B-Cl bond of the shuttlecock molecule can orient either upward or downward.^[29] Recently, the 2D array of SubPcs with both orientations have been imaged also on Ag (001) surface and characterized by tip-enhanced Raman spectroscopy.^[30] Moreover, a reversible orientational switching was achieved by controlling STM conditions so that the SubPc molecules turned all Cl-up or Cl-down orientation depending on the polarity of scanning bias voltages. However, further detailed investigations revealed that the orientational switching was not ascribed to a simple flip-flop change of the axial B-Cl dipoles, since an abrupt switching in the SubPc molecular array occurred even under constant scanning conditions independent of the bias polarity.^[31] Therefore, it has been concluded that the orientational switching of SubPc is not a single molecular event but more intermolecularly correlated phenomenon in the unique arrangement of three-fold SubPc molecules on the four-fold Cu (100) surface. Moreover, the stochastic behavior of flip-flop switching envisages not only statistical thermodynamic interpretation but also quantum consideration of intermolecular entangled states.

Experimental

Macroheterocycles introduced in this review are platinum-tetra(3,5-di-*tert*-butylphenyl)porphyrin (Pt-TBPP) and chloro[subphthalocyaninato]boron(III) (SubPc) as shown in Figure 1(a) and 1(b), respectively. Pt-TBPP was synthesized according to the literature^[32] while SubPc was purchased from Aldrich and purified by sublimation at 573 K in vacuum. Molecular conformations of Pt-TBPP and SubPc were optimized by molecular orbital (MO) calculation based on the density functional theory (DFT) using an Accelrys Material Studio/DMol³ program.

A mechanically polished (001) surface of a Cu single crystal (7×3×0.5 mm³) purchased from Earth Chemical Co.,

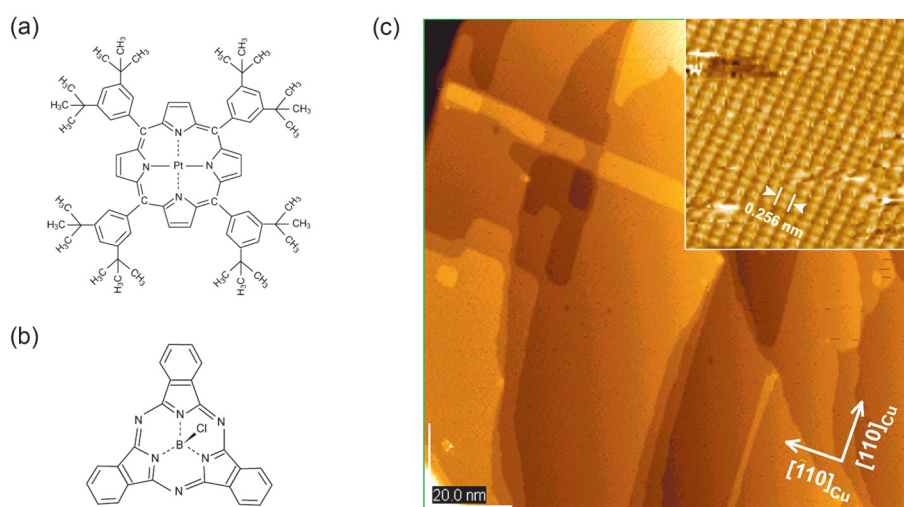


Figure 1. Molecular structures of (a) Pt-TBPP and (b) SubPc. (c) STM image of Cu (001) surface used for deposition of Pt-TBPP and SubPc. The inset indicates high-resolution atomic topography of Cu surface taken at 80 K. Reproduced with permission from Refs.,^[23,29] Copyright 2002, American Chemical Society.

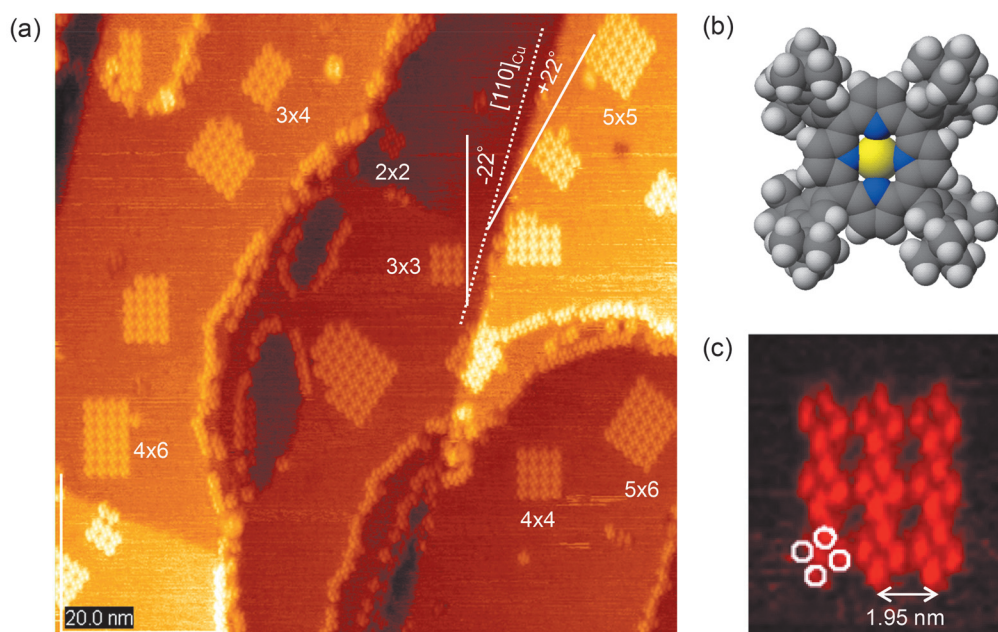


Figure 2. (a) STM image of PtTBPP molecules adsorbed on Cu (001) surface taken at $V_s = 1.00$ V, $I_t = 0.20$ nA at 80 K. (b) Molecular conformation of PtTBPP optimized by DFT calculation. (c) Enlarged image of 3×3 nucleus indicating four-lobed feature of the peripheral *tert*-butyl groups. Reproduced with permission from Ref.,^[23] Copyright 2002, American Chemical Society.

Ltd. was used as substrate. The deposition of macroheterocycles and STM observation were carried out in a multichamber ultrahigh-vacuum STM system (JEOL JSPM-4610). The Cu substrate was mounted on a resistive heater in a preparation chamber ($\sim 3 \cdot 10^{-7}$ Pa) and the surface was atomically cleaned by repeated cycles of Ar⁺ sputtering at 1.0–2.0 keV and annealing at 473–963 K. Figure 1(c) shows a representative STM topograph of the prepared Cu (001) surface indicating the step edges aligning along the $\langle 110 \rangle_{\text{Cu}}$ directions. The inset image shows atomic arrangement in the face-centered (001) lattice of Cu with the spacing of $d_{110} = 0.256$ nm.

After cooling the substrate at room temperature, Pt-TBPP or SubPc loaded on a quartz cell was evaporated onto the Cu surface. Approximately a monolayer of both molecules was deposited by monitoring with a quartz crystal microbalance. The sample was transferred to an analysis chamber ($\sim 2 \cdot 10^{-8}$ Pa) and cooled at ~ 80 K with liquid nitrogen. STM observations were performed using an electrochemically etched tungsten tip.

Results and Discussion

Two-Dimensional Nucleation Growth of Pt-TBPP

The molecular structure of Pt-TBPP optimized by the MO calculation based on DFT is characterized with a four-lobed conformation of the peripheral *t*BP groups, the dihedral angle of which against the porphyrin plane is averagely 63° (Figure 2(b)). Figure 2(a) shows a STM image of the Cu (001) surface deposited with a submonolayer coverage of Pt-TBPP molecules taken at 80 K with the sample voltage $V_s = 1.00$ V and tunneling current $I_t = 0.20$ nA. It indicates that quadrilateral nuclei with different sizes are deposited on the Cu (001) terrace while some edges of the Cu step are decorated with a single-molecular row. An enlarged image shown in Figure 2(c) reveals the four-lobed structure of individual molecules arranged in the nucleus. Note that the typical nuclei are composed of square or rectangular

arrays with the number of molecules of $N = n \times m$. From the smallest nucleus with 2×2 molecules to larger nuclei are found as marked in the Figure. In each nucleus, the Pt-TBPP molecules are arranged in a square lattice with a constant of 1.95 nm, and the side edges of the nuclei orient two directions making angles of $\pm 22^\circ$ with respect to the [110] step of Cu. This orientation is assigned to the epitaxy of Cu(001) Pt-TBPP ($\sqrt{58} \times \sqrt{58}$) as same as that reported for Cu-TBPP on Cu (001).^[18,19]

Such a characteristic adsorption of the Pt-TBPP nuclei is interpreted by thermodynamics of 2D nucleation growth. When the amount of Pt-TBPP molecules covering the Cu surface is decreased, most of molecules are adsorbed on the Cu step and only a few 2D nuclei with a considerably large size are formed on the terrace as shown in Figure 3(a). On the other hand, many nuclei with different sizes are found on the terrace when the deposition coverage is increased as shown in Figure 3(b). It is also noted for the latter case that noisy streaks running parallel to the scanning direction are observed on the surface which corresponds to mobile molecules existing in the 2D gas phase on the Cu surface.^[28] According to the classical nucleation mechanism, the 2D nucleation is driven by the difference of chemical potentials Dm between the 2D gas and nucleus expressed as

$$Dm = kT \ln(1+s) \quad (1)$$

where s is the degree of supersaturation of 2D gas at temperature T . When a 2D nucleus composed of N molecules is formed, the Gibbs free energy change is given by

$$DG = -NDm + g(N) \quad (2)$$

where $g(N)$ is the surface energy replaced with the step energy k which corresponds to the energy increase when

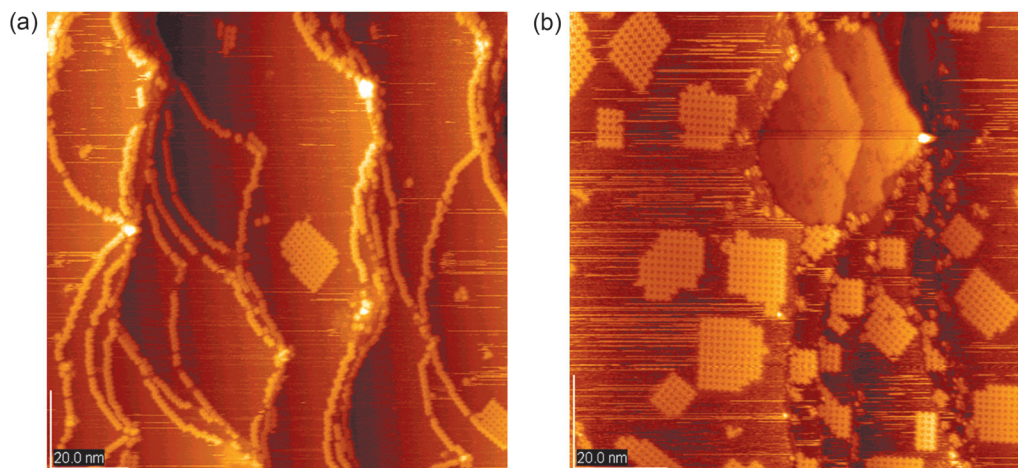


Figure 3. STM images of Pt-TBPP adsorbed on the Cu (001) surface showing single-nucleation growth (a) and multinucleation growth (b). Depending on the amount of adsorbed molecules, the vapor pressure of molecules in the 2D gas phase is low in (a) and high in (b) as seen from the mobile molecules imaged by horizontal streaks on the surface. Reproduced with permission from Ref.,^[23] Copyright 2002, American Chemical Society.

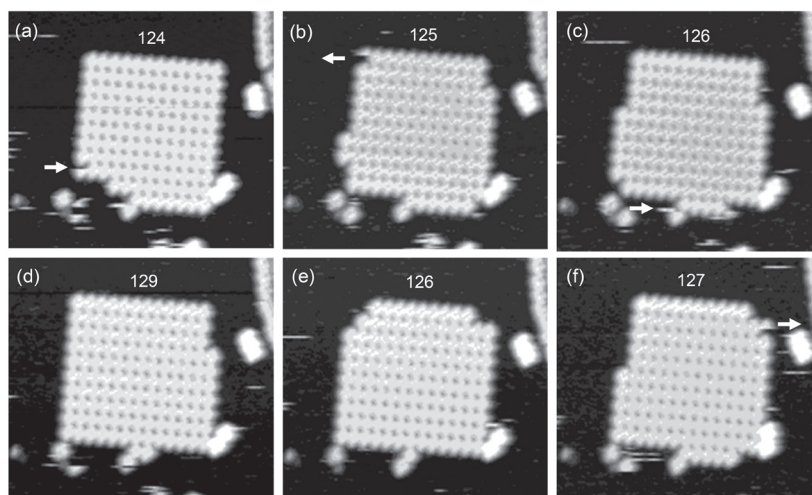


Figure 4. Sequential STM images showing an equilibrium state between 2D gas phase and nucleus. The number of molecules incorporated in each nucleus is shown. Molecular entry and exit at the kink sites are marked with arrows in the image. Reproduced with permission from Ref.,^[23] Copyright 2002, American Chemical Society.

one perimeter of the molecule is exposed to the gas phase. In the simple case of a square nucleus ($N = n \times n$), $g(N)$ increases in proportion to $\dot{O}N$ since $g(N) = 4\dot{O}Nk = 4nk$. In the beginning of nucleation growth, therefore, DG increases with N , and then becomes the maximum value DG^* when the nucleus reaches a critical size n^* ($= \dot{O}N^*$) given by

$$n^* = 2k/Dm. \quad (3)$$

When the nucleus incorporates molecules beyond the critical size, $-NDm$ overcomes $g(N)$, and DG starts to decrease, then the nucleus grows into a 2D aggregate. According to Equation (3), the critical nucleus size increases inversely proportion to Dm so that the lower supersaturation of 2D gas at the reduced molecular coverage results in the larger nucleus growth as shown in Figure 3(a). On the other hand, many small nuclei can grow on the surface

when Dm is increased at the higher 2D gas pressure as shown in Figure 3(b).

Once the nucleation growth reaches an equilibrium with the surrounding 2D gas phase ($\Delta G = 0$), the numbers of molecules incorporating into the nucleus and leaving from it are balanced, therefore, the average size of the nucleus (*i.e.* N) becomes unchanged. Such an equilibrium state was observed in sequential STM images of a nucleus as shown in Figure 4. In the time course of scanning in each image, the tip sometimes encounters to a specific molecule being incorporated into the nucleus (arrows in Figures 4(a) and 4(c)) or leaving from the nucleus (arrows in Figures 4(b) and 4(f)). Such molecular entry and exit usually occurs at the corner of the nucleus step called 'kink' site.

Figure 5 summarizes an energetic change in the 2D nucleation process. An evaporated molecule is attached on the Cu surface by losing the adsorption energy E_a and mobile

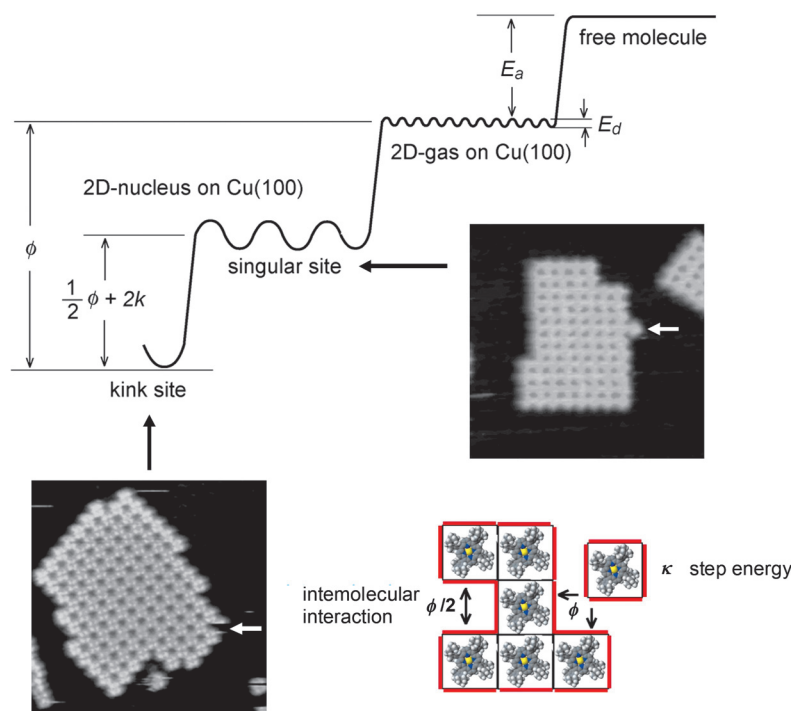


Figure 5. Energy diagram for 2D nucleation process of adsorbed PtTBPP molecules on Cu (001) surface showing kinetic energy of free molecule E_a , potential corrugation of Cu surface E_d , intermolecular interaction energy ϕ and step energy κ . The potential energy decreases by ϕ when one molecule of 2D gas attaches at the kink site, while molecular registry at the singular site increases the energy by $\phi/2 + 2\kappa$. Reproduced with permission from Ref.,^[23] Copyright 2002, American Chemical Society.

in the 2D gas when the kinetic energy of the molecule overcomes the atomic corrugation of the surface potential E_d . When the molecule happens to be incorporated into the kink site, ΔG of the 2D gas-nucleus system decreases by ϕ which corresponds to the intermolecular van der Waals (VDW) interaction between the two peripheries of the incorporating molecule and the molecules at the kink site of the nucleus. In this case, $\gamma(N)$ of the nucleus doesn't change since the number of κ at the nucleus periphery is kept constant. By contrast, if a molecule attaches onto a completed side perimeter of the nucleus called 'singular' site (see inset image in Figure 5), ΔG increases by $\phi/2 + 2\kappa$ with respect to that in the kink site. Therefore, the nucleation is energetically promoted by molecular incorporation at the kink site so that the 2D nuclei grow into square and rectangle shapes.

In order to evaluate those energy parameters, molecular mechanics (MM) and molecular dynamics (MD) calculations were carried out using the universal force field^[33] for the PtTBPP molecule and the nuclei adsorbed on the Cu (100) surface constructed with $20 \times 20 \times 1$ unit cells. E_a for an isolated PtTBPP molecule was calculated to be $5.3 \text{ kcal}\cdot\text{mol}^{-1}$. By varying the aggregating shapes of a nucleus with $N=4$, ϕ and κ were estimated to be 16.6 and $1.1 \text{ kcal}\cdot\text{mol}^{-1}$, respectively. The obtained value of ϕ is considerably higher than the energy increase of $\phi/2 + 2\kappa = 10.5 \text{ kcal}\cdot\text{mol}^{-1}$ at the singular site, demonstrating the favourable molecular entry into the kink site. The present experimental observations molecularly visualize the 2D nucleation growth of PtTBPP molecules, and its simple thermodynamic interpretation well explains

the self-assembling process of the macroheterocycles on the surface.

Stochastic Flip-flop Switching of SubPc Array

In the second section, STM-induced switching of macroheterocycle molecules is presented for SubPc arrays adsorbed on Cu surface. Figure 6(a) shows a typical STM image of as-deposited SubPc molecules on Cu (001) taken at 78 K under scanning parameters of $V_s = -1.30 \text{ V}$ and $I_t = 0.20 \text{ nA}$. The adsorbed SubPc monolayer is imaged as a dot array with a square lattice the direction of which aligns parallel to the [110] step of the Cu surface. Each dot arranged in the lattice is regarded as an individual molecule based on the consistency between the square lattice constant of $\sim 1.3 \text{ nm}$ and the molecular dimension of SubPc. Since this lattice constant is five times as large as d_{110} ($=0.256 \text{ nm}$) of Cu, the SubPc monolayer array is formed by the epitaxy of Cu(001)SubPc(5 \times 5) on the Cu surface. However, it should be noted that each molecular dot appears in high (bright) or low (dark) topography, and they randomly arrange as shown in the enlarged image in Figure 6(b). As shown in Figure 6(c), the profile along the line marked with double arrows in Figure 6(a) indicates the height difference in the high and low topography with respect to the Cu surface exposed by a void of a single molecule.

Surprisingly, such a random array of high and low topography in the as-deposited monolayer changes to homogeneous images with all-high or all-low topography depending on V_s as shown in Figure 7(a) and 7(b),

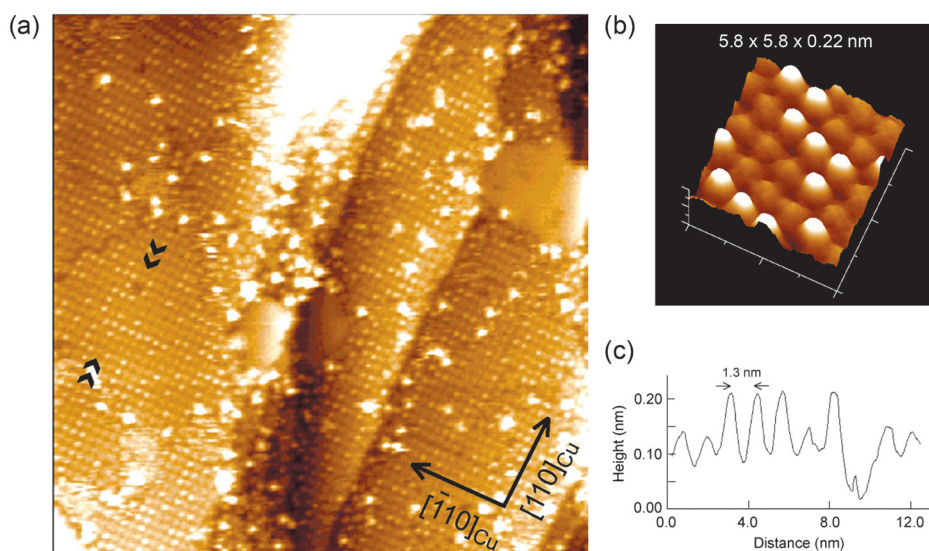


Figure 6. (a) STM image of SubPc molecular array as-adsorbed on Cu (001) taken at $V_s = -1.30$ V, $I_t = 0.20$ nA (image area, 60×60 nm). (b) Enlarged image of SubPc array showing high and low topography. (c) Height profile along the line marked with double-arrows in (a). Reproduced with permission from Ref.,^[29] Copyright 2002, American Chemical Society.

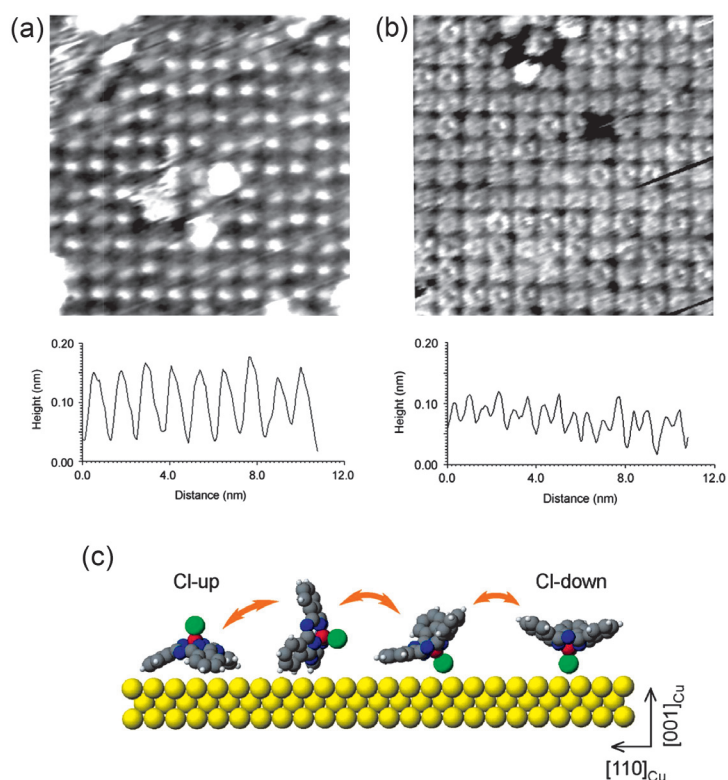


Figure 7. STM images and height profiles of SubPc molecular arrays on Cu (001) showing all Cl-up (a) and all Cl-down (b) orientations taken at $V_s = +1.30$ V, $I_t = 0.20$ nA and $V_s = -1.30$ V, $I_t = 0.20$ nA, respectively. (c) Schematic diagram for flip-flop switching of SubPc molecule between Cl-up and Cl-down orientations on Cu (100). Reproduced with permission from Ref.,^[29] Copyright 2002, American Chemical Society.

respectively. When the bias voltage is changed to positive at $V_s = +1.30$ V in the former case, all the molecular dots appear with a single apex with a height of > 0.1 nm. On the other hand, the height profile changes to less-corrugated topography and each molecule is imaged with a donut-like shape when the bias is returned to negative at $V_s = -1.30$ V. These changes in high or low topography can be ascribed to orientational switching of the SubPc molecule with its Cl head upward or downward, respectively, as schematically depicted in Figure 7(c). The steep apex in the former topography well coincides with a protrude of the Cl-B bond upward (Cl-up) while the latter donut-like topography corresponds to a concave of the molecule with the Cl-B bond downward (Cl-down).

In the previous STM study, a three-lobed topography corresponding to the three-fold isoidoline moieties of the SubPc molecule with the Cl-down orientation was imaged on the Si(111) surface.^[27] By contrast, the present donut-like image suggests that the Cl-down molecules rotate in the square lattice array on Cu (001). A similar molecular rotation has been reported for hexa-*tert*-butyl decacyclene deposited on Cu (001). The six-fold *tert*-butyl groups plays a role of molecular bearing and the rotation can occur at room temperature only for a specific molecule which is disengaged from the closely packed array in the hexagonal lattice.^[34] In the present case, the downward B-Cl axis probably acts as a molecular rotor, but the rotation occurs for all the Cl-down molecules arranged in the square lattice array at liquid N_2 temperature. Although the inconsistency between the square packing and the three-fold symmetry of SubPc would give a degree of freedom for the molecular rotation, it envisages another contribution of quantum effects in the entangled molecular array as discussed later.

Transient switching between the Cl-up and Cl-down molecules are reversely observed in sequential images taken by changing the scanning parameters. In most

of cases, the initial scanning gives an image of randomly arranged Cl-up and Cl-down molecules as shown in Figure 8(a) which is typically obtained at negative $V_s (= -1.30$ V) and relatively low $I_t (= 0.15$ nA). After the same sample area was scanned a few times at higher $I_t (= 0.20$ nA) while keeping V_s constant, the Cl-up molecules turned upside down, and all the molecule were switched to the Cl-down (Figure 8(b)). When the sample voltage was changed to positive ($V_s = +1.30$ V) in the next scan, all the molecules turned to the Cl-up orientation (Figure 8(c)). This all Cl-up state was further scanned by setting V_s negative again so that the subsequent images exhibit transient switching from the Cl-up to Cl-down states as shown in Figures 8(d) and 8(e). In Figure 8(d), the image of individual molecules is blurred probably due to the molecular motion in the transient state. Then, each molecule becomes discriminative in the square array in Figure 8(e) in which most of molecules turned to the Cl-down but some of them appear with a two-lobed feature. It suggests that those molecules are inclined with the Cl-head facing down and two of the three isoidoline moieties give two-lobed protrudes (see Figure 7(c)). In this series of transient images, it should be noted that the sites of these two-lobed molecules (Figure 8(e)) are almost consistent with those of the Cl-up molecules in the initial image (Figure 8(a)). It is so miraculous as to envisage some memory effect existing in the course of sequential switching.

The above-mentioned switching of SubPc depending on V_s simply reminds us that the flip-flop change may arise from the polarity of the axial B-Cl bond. However, the Cl-down (Cl-up) orientation at the negative (positive) bias of V_s , is not consistent with the dipole direction of B(δ^+)-Cl(δ^-) since the negatively charged Cl head ought to orient down to the positively biased Cu surface. Not only this inconsistency of the switching polarity is unexplainable, the flip-flop switching is also observed during continuous

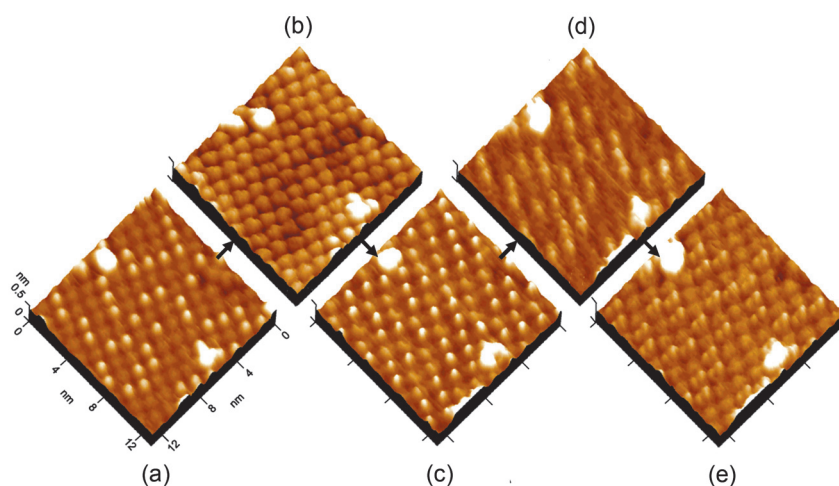


Figure 8. A series of STM images showing reversible flip-flop switching of SubPc on Cu (001). (a) Initial image showing randomly distributed Cl-up and Cl-down molecules taken at $V_s = -1.30$ V, $I_t = 0.15$ nA. (b) Switching to all Cl-down image taken after a few scans at $V_s = -1.30$ V, $I_t = 0.20$ nA. (c) Switching to all Cl-up orientation by changing the condition at $V_s = +1.30$ V, $I_t = 0.20$ nA. (d) Transient state between Cl-up and Cl-down orientations taken by returning to negative bias condition ($V_s = -1.30$ V, $I_t = 0.20$ nA). (e) Subsequent transient state returning to all Cl-down orientation taken at $V_s = -1.30$ V, $I_t = 0.20$ nA. Reproduced with permission from Ref.,^[29] Copyright 2002, American Chemical Society.

scans under constant conditions of V_s and I_t . Figure 9 shows sequential STM images taken from the same sample area ($60 \times 36 \text{ nm}^2$) at $V_s = -1.30 \text{ V}$, $I_t = 0.20 \text{ nA}$ in which the tip scanning line is from left to right. The first scanning (Figure 9(a)) gives a uniform topography image of all Cl-down molecules and some ad-molecules are found piling on top of the monolayer. In the second scan (Figure 9(b)), the all Cl-down state is still imaged up to the scanning line marked with an arrow, but it suddenly switched to the mixture state with Cl-up and Cl-down molecules. In the third scan (Figure 9(c)), this mixture state is observed in the scanning area before the marked line suggesting that the switching from the all-Cl-down to the mixture state has happened at once in the previous scan. At the marked line in Figure 9(c), the mixture state again changes to the all Cl-down orientation in the scanning area after the marked line. In the fourth scan (Figure 9(d)), the all-Cl-down state is kept but the scanning after the marked line swept off the ad-molecules. Finally, the fifth scan (Figure 9(e)) gives rise to very homogeneous topography composed of the all Cl-down molecules. In the course of this sequential imaging, it is noted that the switching between the all-Cl-down and mixture states always occurs at almost the same scanning line. In the vicinity of this scanning line, there is a high protrude which is probably an etched residue of the Cu surface. From this finding, we assume that an unexpected close approach (or contact) of the STM tip to the surface caused by this protrude may cause an unexpected tip turbulence beyond the feedback control which triggers the orientational switching of all molecules in the scanning area (or in the whole sample area). It strongly suggests that the observed switching is not a single-molecular event, but more intermolecularly correlated phenomena.

In order to elucidate the switching behavior observed in Figure 9, the energy difference between the Cl-up (ϕ_{up}) and Cl-down (ϕ_{down}) molecules on the Cu (001) surface was evaluated with the DFT-MO and MM calculations. For the calculation, the fcc lattice of the Cu (001) surface was constructed and one SubPc molecule was made contact

onto the Cu (001) surface with different angles of the B-Cl bond while the distance between the molecule and surface was fixed to their VDW radii. As a result, the total energy difference $\phi_{\text{up}} - \phi_{\text{down}} = 8.3 \text{ kcal}\cdot\text{mol}^{-1}$ obtained by DFT-MO indicates that the Cl-down is more stable than the Cl-up although the VDW interaction of the Cl-up molecule with the Cu surface is higher by $3.7 \text{ kcal}\cdot\text{mol}^{-1}$ than the Cl-down molecule. According to statistical thermodynamics, the order parameter $s = 2r - 1$, where r is the probability of the Cl-down orientation, is expressed as

$$s = \frac{\exp\left[\left(\phi_{\text{up}} - \phi_{\text{down}}\right) / kT\right] - 1}{\exp\left[\left(\phi_{\text{up}} - \phi_{\text{down}}\right) / kT\right] + 1} \quad (4)$$

The evaluated value of $\phi_{\text{up}} - \phi_{\text{down}}$ results in $s \cong 1$ indicating that the SubPc molecules are in the completely ordered state with all-Cl-down orientation as schematically shown in Figure 10(a).

Although the above statistical estimation explains the favourable orientation of the all Cl-down state, the question remains to be considered why the flip-flop switching occurs from this stable “all Cl-down” to the “Cl-up” orientation under continuous scans at a constant condition. Since an unexpected tip turbulence is suggested as a plausible trigger of the switching in Figure 9, the tip-sample distance was intentionally changed by controlling I_t . Figure 10(b) shows a change in STM images observed with increasing I_t at constant $V_s = -1.20 \text{ V}$. The as-adsorbed monolayer is in the mixture state of Cl-up and Cl-down orientations. In this initial mixture state observed at $I_t = 0.15 \text{ nA}$, the ratio of the Cl-up molecules to the Cl-down ones is about 2:3 which is almost maintained at $I_t = 0.25 \text{ nA}$ (Figure 10(c)). However, the ratio of the “Cl-up” molecules is apparently increased when the tip-sample distance is shortened by increasing I_t to 0.35 nA (Figure 10(d)), then the molecular array is finally disordered at $I_t = 0.45 \text{ nA}$ as is seen from the noisy streaks in Figure 10(e). It suggests that the excessive tip approach at high I_t triggers a rearrangement of the molecular array

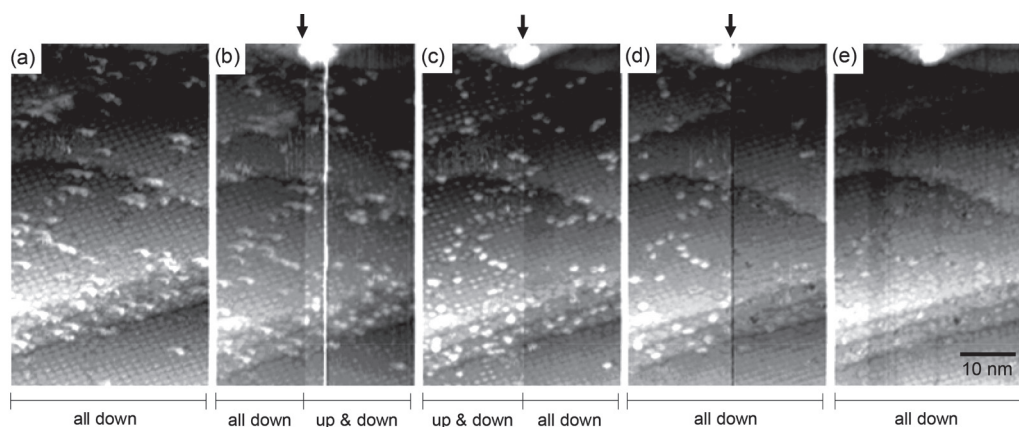


Figure 9. Changes in STM images taken by continuous scanning at $V_s = -1.30 \text{ V}$, $I_t = 0.20 \text{ nA}$ (tip scanning line is from left to right). (a) The first scan indicating a monolayer composed of all “Cl-down” molecules and some ad-molecules on top of it. (b) The second scan showing a sudden change from all Cl-down to the mixture state of Cl-up and Cl-down at the scanning line marked with arrow. (c) The third scan showing a return to all Cl-down after the marked scanning line. (d) The next scan keeping all Cl-down orientation but sweeping ad-molecules on top of the monolayer at the marked line. (e) The last scan resulting in a uniform monolayer composed of all Cl-down molecules. Reproduced with permission from Ref.,^[31] Copyright 2005, Elsevier.

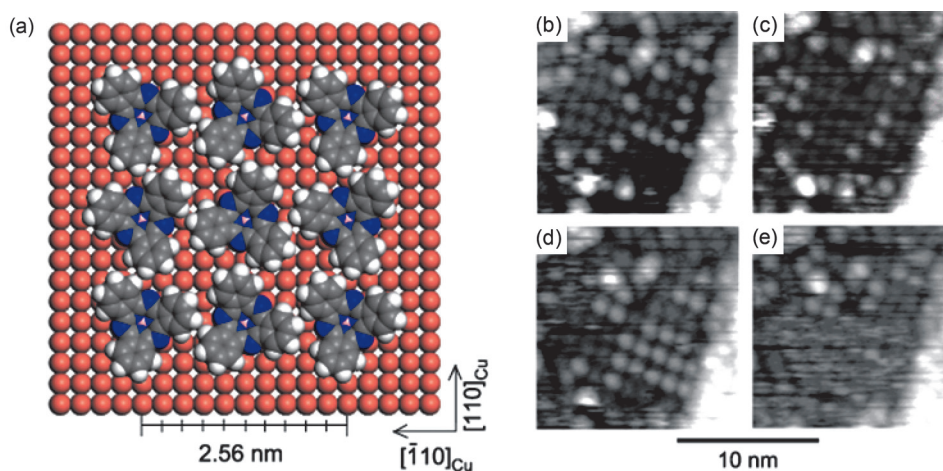


Figure 10. (a) Schematic model for close-packed array of SubPc molecules in a square unit-cell ($a = b = 2.56$ nm) taking Cu(100) SubPc(10×10) epitaxy. Change of STM images in the mixture state of Cl-up and Cl-down molecules with increasing I_t from 0.15 (b) to 0.25 (c), 0.35 (d) and 0.45 nA (e) at constant $V_s = -1.20$ V. Reproduced with permission from Ref.^[31] Copyright 2005, Elsevier.

which gives a clue for the observed flip-flop switching of SubPc molecules.

Conclusions

This review summarized the author's studies on STM imaging of macroheterocycle molecules deposited on Cu surface under ultra-high vacuum. In the first section, 2D nucleation growth of Pt-TBPP molecules was molecularly visualized and classical thermodynamics was introduced to model the self-assembling process to the molecular crystals. It demonstrated that the chemical potential of the adsorbed molecule depending on the supersaturation of the 2D gas phase determined the critical size of nuclei. The estimated intermolecular interaction and step energy revealed that the adsorbed molecules were incorporated to the kink site resulting in the growth of nuclei into square or rectangular shapes. The direct observation of the attachment and detachment of a molecule at the kink site also visualized the equilibrium state between the 2D gas and solid phases.

In the second section of the review, STM-induced single-molecular switching was presented for SubPc molecules on the Cu surface. The observed switching was ascribed to the flip-flop change between the Cl-up and Cl-down orientations. However, the dipole orientation of the axial B-Cl bond was inconsistent with the polarity of the bias voltage between the tip and sample. Moreover, the switching from the initial mixture state with Cl-up and Cl-down molecules to the all-Cl-down array was observed under sequential scans at a constant bias. A plausible trigger of the switching was attributed to unexpected tip approach caused by surface protrudes or a change of scanning conditions. These findings suggested that the observed switching was not a single-molecular event but related to an intermolecularly correlated phenomenon among the SubPc molecules arranged in the 2D array. The unique asymmetric geometry of the three-fold SubPc molecule on the four-fold square lattice of Cu might play a role for the stochastic switching

in the molecular array. It is assumed that the molecular packing in this symmetry-mismatched epitaxy could give rise to entangled intermolecular interactions over the monolayer lattice. Once the molecular arrangement is disturbed by unexpected tip approach, the molecular array might be restructured to a different entangled state. It reminds us that the observed stochastic switching of SubPc is not interpreted by a classical flip-flop event but more concerns quantum-based phenomena.

Acknowledgements. This work was supported by the PRESTO program by Japan Science and Technology Agency (JST), and by the Photonics Materials program by the Venture Business Laboratory of Kobe University.

References

1. Uyeda N., Kobayashi T., Suito E., Harada Y., Watanabe M. *J. Appl. Phys.* **1972**, *43*, 5181–5189.
2. Ishizuka K., Uyeda N. *Acta Cryst.* **1977**, *A33*, 740–749.
3. Uyeda N., Kobayashi T., Ishizuka K., Fujiyoshi Y. *Chemica Scripta* **1978–79**, *14*, 47–61.
4. Unwin P.N.T., Henderson R. *J. Mol. Biol.* **1975**, *94*, 425–440.
5. Fujiyoshi Y., Kobayashi T., Ishizuka K., Uyeda N. *Ultramicroscopy* **1980**, *5*, 459–468.
6. Binnig G., Rohrer H., Gerber Ch., Weibel E. *Phys. Rev. Lett.* **1983**, *50*, 120–123.
7. Binnig G., Quate C.F., Gerber Ch. *Phys. Rev. Lett.* **1986**, *56*, 930–933.
8. Zhang L., Sakai T., Sakuma N., Ono T., Nakayama K. *Appl. Phys. Lett.* **1999**, *75*, 3527–3529.
9. Hartmann U. *J. Appl. Phys.* **1988**, *64*, 1561–1564.
10. Hansma P.K., Drake B., Marti O., Gould S.A., Prater C.B. *Science* **1989**, *243*, 641–643.
11. Betzig E., Trautman J.K., Harris T.D., Weiner J.S., Kostelak R.L. *Science* **1991**, *251*, 1468–1470.
12. Eigler D.M., Schweizer E.K. *Nature* **1990**, *344*, 524–526.
13. Bartels L., Meyer G., Rieder K.H. *Phys. Rev. Lett.* **1997**, *79*, 697–700.
14. Avouris P. *Acc. Chem. Res.* **1995**, *28*, 95–102.

15. Sedona F., Di Marino M., Forrer D., Vittadini A., Casarin M., Cossaro A., Floreano L., Verdini A., Sambri M. *Nat. Mater.* **2012**, *11*, 970–977.
16. Zhao A., Li Q., Chen L., Xiang H., Wang W., Pan S., Wang B., Xiao X., Yang J., Hou J.G. *Science* **2005**, *309*, 1542–1544.
17. Jiang N., Zhang Y.Y., Liu Q., Chen Z.H., Deng Z.T., Du S.X., Gao H.J., Beck M.J. *Nano Lett.* **2010**, *10*, 1184–1188.
18. Jung T.A., Schlittler R.R., Gimzewski J.K., Tang H., Joachim C. *Science* **1996**, *271*, 181–184.
19. Jung T.A., Schlittler R.R., Gimzewski J.K. *Nature* **1997**, *383*, 696–698.
20. Moresco F., Meyer G., Rieder K.H. *Phys. Rev. Lett.* **2001**, *86*, 672–675.
21. Yokoyama T., Yokoyama S., Kamikado T., Okuno Y., Mashiko S. *Nature* **2001**, *413*, 619–621.
22. Yokoyama T., Yokoyama S., Kamikado T., Mashiko S. *J. Chem. Phys.* **2001**, *115*, 3814–3818.
23. Yanagi H., Mukai H., Ikuta K., Shibutani T., Kamikado T., Yokoyama S., Mashiko S. *Nano Lett.* **2002**, *2*, 601–604.
24. Gimzewski J.K., Joachim C. *Science* **1999**, *283*, 1683–1688.
25. Donhauser Z.J., Mantooth B.A., Kelly K.F., Bumm L.A., Monnell J.D., Stapleton J.J., Prince Jr. D.W., Rawlett A.M., Allara D.L., Tour J.M., Weiss P.S. *Science* **2001**, *292*, 2303–2307.
26. Weitemeyer A., Klisch H., Wöhrle D. *J. Org. Chem.* **1995**, *60*, 4900–4904.
27. Yanagi H., Schlettwein D., Nakayama H., Nishino T. *Phys. Rev. B* **2000**, *61*, 1959–1964.
28. Berner S., Brunner M., Ramoino L., Suzuki S., Güntherodt H.-J., Jung T.A. *Chem. Phys. Lett.* **2001**, *348*, 175–181.
29. Yanagi H., Ikuta K., Mukai H., Shibutani T. *Nano Lett.* **2002**, *2*, 951–955.
30. Whiteman P.J., Schultz J.F., Porach Z.D., Chen H., Jiang N. *J. Phys. Chem. Lett. C* **2018**, *122*, 5489–5495.
31. Yanagi H., Ikuta K. *Surf. Sci.* **2005**, *581*, 9–16.
32. Ponomarev G.V., Yashunskii D.V., Moskovkin A.S. *Chem. Heterocycl. Compd.* **1997**, *33*, 271–275.
33. Rapeé A.K., Casewit C.J., Colwell K.S., Goddard W.A., Skiff W.M. *J. Am. Chem. Soc.* **1992**, *114*, 10024–10035.
34. Gimzewski J.K., Joachim C., Schlittler R.R., Langlais V., Tang H., Johannsen I. *Science* **1998**, *281*, 531–533.

Received 24.07.2019

Accepted 29.09.2019